CLIMATOLOGY

Combined high- and low-latitude forcing of East Asian monsoon precipitation variability in the Pliocene warm period

Yichao Wang[1], Huayu Lu[1]*, Kexin Wang[1], Yao Wang[1], Yongxiang Li[2], Steven Clemens[3], Hengzhi Lv[1], Zihan Huang[1], Hanlin Wang[1], Xuzhi Hu[2], Fuzhi Lu[1], Hanzhi Zhang[1]

East Asian monsoon variability in the Pliocene warm world has not been sufficiently studied because of the lack of direct records. We present a high-resolution precipitation record from Pliocene fluvial-lacustrine sequences in the Weihe Basin, Central China, a region sensitive to the East Asian monsoon. The record shows an abrupt monsoon shift at ~4.2 million years ago, interpreted as the result of high-latitude cooling, with an extratropical temperature decrease across a critical threshold. The precipitation time series exhibits a pronounced ~100–thousand year periodicity and the presence of precession and half-precession cycles, which suggest low-latitude forcing. The synchronous phase but mismatched amplitudes of the East Asian monsoon precipitation proxy and eccentricity suggest a nonlinear but sensitive precipitation response to temperature forcing in the Pliocene warm world. These observations highlight the role of high- and low-latitude forcing of East Asian monsoon variations on tectonic and orbital time scales.

INTRODUCTION

Climate change in most parts of Asia is governed by the monsoonal circulation. However, how the East Asian monsoon responded to global warming, especially on orbital time scales, is not well understood, even for the Late Pleistocene (*1*, *2*), and even less so for the Pliocene (*3*). The Pliocene saw a notable transition from relatively warm conditions to widespread cooling and more extensive Arctic ice sheets in the Pleistocene (*4*–*6*). Northern Hemisphere glaciation (NHG) developed as a gradual transition, with the onset at ~3.6 million years (Ma) before present (BP) (*7*) and an intensification at ~2.7 Ma BP (*8*). Before ~3.6 Ma BP, the high latitudes of the Northern Hemisphere were substantially warmer than today and there were no widespread Arctic ice sheets (*9*, *10*); however, after ~3.6 Ma BP, Arctic ice sheets began to expand, accompanied by a gradual cooling trend (*7*, *11*, *12*). Understanding the variability and driving mechanisms of the East Asian monsoon circulation before and after the ice sheet expansion in the Pliocene may help elucidate the drivers of East Asian monsoon variability under future warming scenarios.

Here, we report a high-resolution Pliocene record of East Asian monsoon variations from the Weihe Basin, which preserves an outstanding record of Cenozoic terrestrial paleoclimate variations [Fig. 1, A and B; (*13*–*16*)]. The region today has a semihumid monsoon–dominated climate. A continuous sequence of Cenozoic fluviolacustrine deposits with rich assemblages of mammalian fossils is preserved in the southeastern Weihe Basin (Fig. 1B). We investigated the newly found Changgoucun (CGC) sedimentary sequences (34°18′N, 109°30′E), which are located in the southeastern margin of the Weihe Basin (Fig. 1C), and we obtained the first continuous, high-resolution time series of East Asian monsoon precipitation variability from the Late Miocene to the Early Pleistocene. The record enables us to examine precipitation regimes before and after the initial expansion of the Arctic ice sheets. In particular, the previously unidentified record helps determine (i) whether the monsoon was paced by eccentricity in a warm world and (ii) the possible forcing mechanisms of the East Asian monsoon variability on tectonic through orbital time scales in the Pliocene.

RESULTS

Chronology

Two mammalian fossil–bearing layers were observed in the CGC sections (Fig. 2). One is a Bovidae gen. et sp. indet (fig. S4) found in the middle part of the sedimentary sequence in 2017, which was determined to indicate a Late Miocene age or younger (by Z. Zhang, Chinese Academy of Sciences). The other fossil, of *Hipparion* sp., was found in the upper part of the section (*17*), indicating an age ranging from the Late Miocene to the Pliocene. In addition, the CGC sequence conformably underlies an Early Pleistocene loess-paleosol sequence (Fig. 1D), indicating that the CGC is older than ~2.6 Ma BP. In summary, the fluviolacustrine sequence is older than Early Pleistocene and younger than Late Miocene, which provides an age range between ~7 and ~2.6 Ma BP; hence, its age is equivalent to that of the eolian Red Clay deposit in North China (*18*–*20*).

Virtual geomagnetic pole (VGP) latitudes calculated from 414 reliable characteristic remanent magnetization (ChRM) directions (table S1) were used to construct the magnetic polarity stratigraphy that comprises nine normal and eight reversed polarity intervals (Fig. 2). Twelve samples that showed unmatched inclination and declination data were used only as second-order determinants of polarity. The durations of the three major normal polarity zones and the two major reversed polarity zones enabled a detailed correlation of the polarity sequence with the geomagnetic polarity time scale (GPTS) (*21*), from the Late Miocene to the Early Pleistocene, with the additional constraint of the biostratigraphy. Both the normal and reversed polarity intervals matched well with all of the GPTS polarity subzones within the age interval from chrons C3An to C2An. This provided an independent and detailed time scale between 6.73

[1]School of Geography and Ocean Science, Nanjing University, Nanjing 210023, China. [2]School of Earth Sciences and Engineering, Nanjing University, Nanjing 210023, China. [3]Earth, Environmental, and Planetary Sciences, Brown University, Providence, RI 02912, USA.
*Corresponding author. Email: huayulu@nju.edu.cn

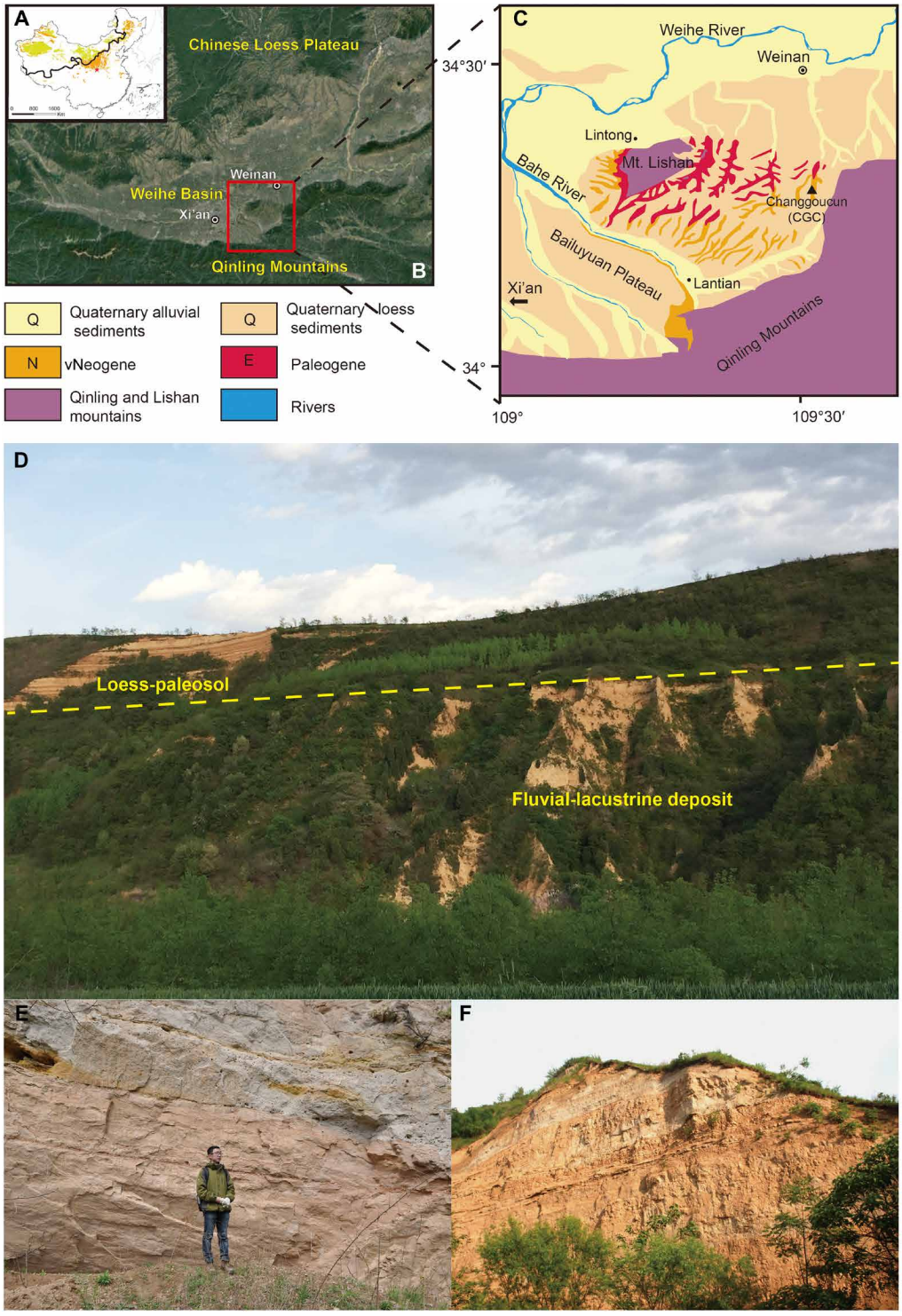

Fig. 1. Location, regional geological settings, and investigated sections. (**A**) The study area is located in the monsoon-dominated semihumid region of China. The black solid line is the 400-mm isohyet, which separates the monsoon semiarid and semihumid regions, and the red star shows location of the study area in China. (**B**) Location of the Weihe Basin; the rectangle corresponds to the area of the geological map shown in (C). (**C**) Geological map with localities mentioned in the text. (**D**) The major lithology of the upper part of the CGC sequence is thick yellowish-red sandy mudstone with interbedded yellow conglomeratic sand layers, or occasionally gravel layers. The loess-paleosol sequence is seen above the dashed line. (Photo credit: Yichao Wang, School of Geography and Ocean Science, Nanjing University.) (**E**) The middle part of the CGC sequence is mainly composed of three conglomeratic sand and gravel layers interbedded with two reddish-brown mudstone layer. (Photo credit: Huayu Lu, School of Geography and Ocean Science, Nanjing University.) (**F**) The lithology of the lower part mainly comprises frequent alternations of fine-grained massive sandy mudstone, conglomeratic massive sandstone, and massive or crudely bedded sand clast-supported conglomerate. (Photo credit: Yichao Wang, School of Geography and Ocean Science, Nanjing University.)

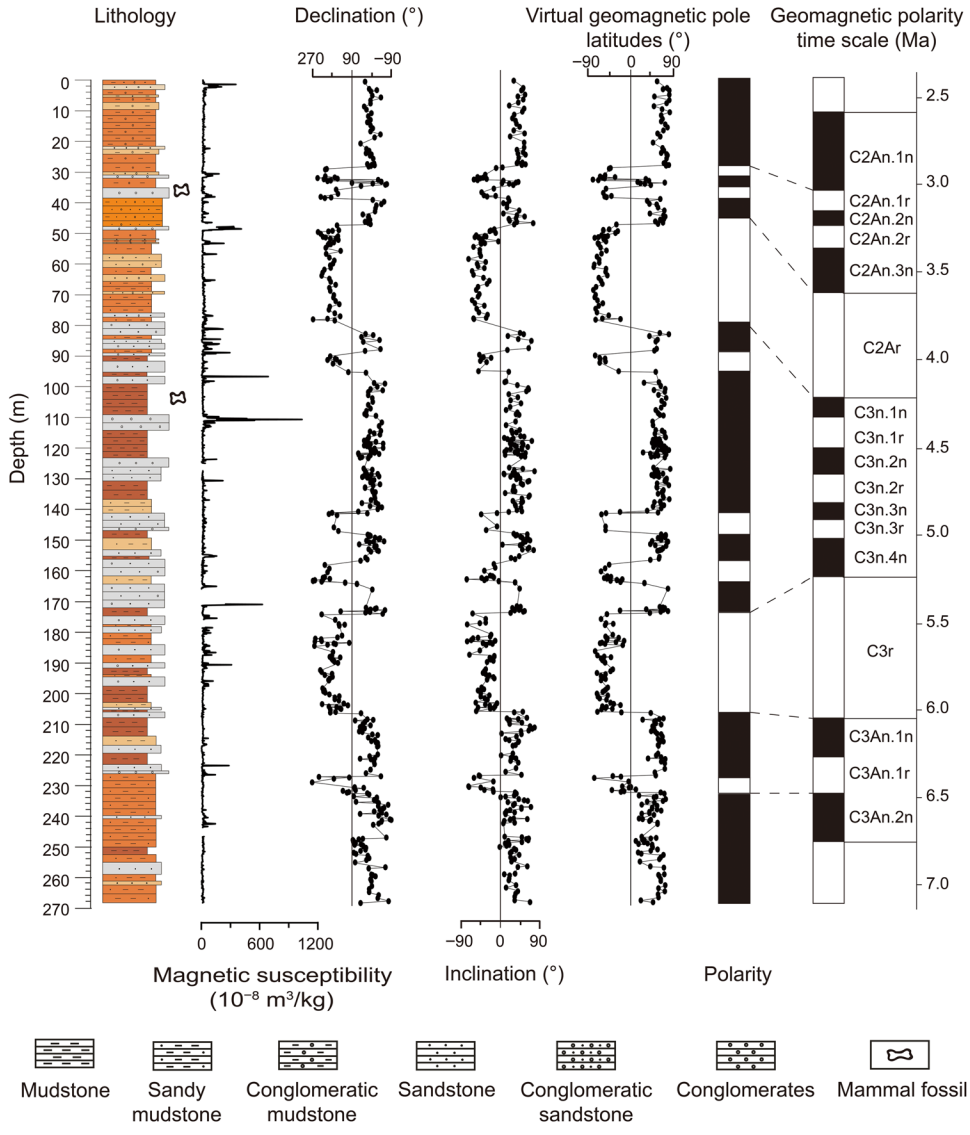

Fig. 2. Lithostratigraphy, magnetostratigraphy, and magnetic susceptibility of the CGC sequence and correlation with the geomagnetic polarity time scale (*21*). High magnetic susceptibility values correlate with coarse-grained deposits, reflecting flooding intensity, and the type and quantity of the magnetic minerals in the source area may influence the magnetic susceptibility variations, although they are not discussed in detail in this paper.

and 2.58 Ma BP. Subsequently, the age of each sampling level was estimated by piecewise linear interpolation between age control points, enabling the sediment accumulation rate of each polarity interval to be obtained (fig. S2). The derived average sediment accumulation rate of the entire CGC sequence is 64.7 m/Ma, close to that of the underlying Late Miocene Bahe fluviolacustrine sequence 30 km away, which has average sediment accumulation rates of 40 to 60 m/Ma (*15*). Although the average sediment accumulation rates remain relatively constant, the interval corresponding to chron C3n.2n suggests an increase in sediment accumulation rate (fig. S2), likely reflecting the combined influences of the migration of the alluvial fan depocenter, long-term climate change, and a lateral facies shift among the various sampling outcrops (see the detailed analysis in the Supplementary Materials, part 2).

East Asian monsoon precipitation variations during the Pliocene

Similar to the sedimentary facies and structure of the Late Miocene Bahe Formation in the Weihe Graben (*14*, *15*), the CGC sequence is composed of frequent alternations between mudstone and siltstone to conglomeratic sandstone, containing continuous alluvial fan and flood plain deposits, which indicate periodic hydrodynamic changes. There are three exposures along the Changgou gully, with a total vertical thickness of 287 m (Fig. 1 and the Supplementary Materials, part 1). The sections dip 165° to 160° with angles between 8°and 13°. Details of the sedimentary facies and structures are presented in the Supplementary Materials (part 1); the CGC sequence is a nearly continuous deposit without obvious erosive surfaces or angular unconformities. The conglomerate to sandy sediments are fluvial channel deposits, and the sandy mudstone, mudstone, and clay deposits are crevasse splays, indicating sheet floods and floodplains with paleosol development. These deposits contain obvious carbonate accretions and nodules, as well as mottling, indicating subaerial exposure of sediment surfaces with evaporation and weathering. In addition, clay deposits and laminated dark red mudstone indicate a shallow lake deposit within the CGC sequence. Together, the CGC

sedimentary sequence demonstrates nearly continuous sediment accumulation in a distal alluvial fan setting with anastomosing low-energy river channels. Intermittent increased runoff and high-energy floods events transported coarser sediments and eroded the channels, as indicated by gravels and/or sandy sediments. Our sampling sites show that the hydrological system varied substantially, from large channels to flood basin ponds, to virtual nondeposition where mature paleosols developed.

The >63-μm coarse-particle content (sand fraction) (Fig. 3A) is the main grain size component of the samples, and therefore, it is positively correlated with the mean grain size (Fig. 3B). Under these circumstances, the grain size variations likely reflect changes in the hydrodynamic strength of surface runoff, with coarser grain size distributions indicating stronger streamflow and increased monsoon precipitation, and vice versa. The magnetic susceptibility of the CGC sequence, determined by the content, size, and type of the magnetic grains in sediments (*22*), is an indicator of alternations in the depositional environment, sediment provenance, and partly of changes in sediment grain size distributions (Fig. 2). The magnetic susceptibility record suggests changes in flood intensity and in the magnetic mineral assemblages in the source area, manifested as cyclic variations; it has a relatively complex pattern that we do not discuss here (Fig. 2 and fig. S8).

The mean grain size and the >63-μm fraction show similar patterns in terms of the amplitude and frequency of variations during the Late Miocene to the earliest Pleistocene, with large-amplitude fluctuations before ~4.2 Ma BP and with damped fluctuations thereafter (Fig. 3, A and B). For example, the >63-μm fraction varies between 0 and 90% before ~4.2 Ma BP but between 10 and 70% thereafter (Fig. 3A). These changes suggest a trend of decreasing hydrodynamic strength, hence monsoon precipitation, after ~4.2 Ma BP (Fig. 3).

To further investigate climate variations on orbital time scales, we performed wavelet analysis and spectral analysis of the mean grain size time series, with a sampling interval of 1.6 thousand years (ka) (~10-cm resolution). The distribution of variance with frequency indicates a consistent ~100-ka periodicity throughout the interval from 6.73 to 2.58 Ma BP (Fig. 3, A and B, and fig. S5, A and B). The continuous wavelet analysis results reveal that the variation of mean grain size is dominated by the ~100-ka Earth orbital eccentricity cycle (95- and 124-ka signatures being broadly delineated), with a weak contribution from orbital obliquity (54- and 37-ka cycles) and precession (19-ka cycle) (Fig. 4A). To test whether these orbital signals in the spectrum were robust, we performed spectral analysis (using both REDFIT and Blackman-Tukey methods) of the grain size time series for the intervals of 6.73 to 3.6 Ma BP, 3.6 to 2.58 Ma BP, and 6.73 to 2.58 MaBP (the entire record). The age of ~3.6 Ma BP was chosen as a breakout age for the grain size time series because it corresponds to the onset of NHG, accompanied by a prominent cooling trend (*8*, *11*, *12*). The REDFIT results (Fig. 4B) show that ~100-, 40-, and ~20-ka orbital cycles are present within the grain size record during 6.73 to 2.58 Ma BP, with confidence levels higher than 95%, and that the ~100-ka cycle has the strongest spectral power. The 19-ka and 12-ka cycles are potential responses to precession and half-precession forcing; the 54- and 37-ka cycles may represent the main cycles of obliquity (54 and 41 ka); and the 124- and 99-ka cycles likely represent the short eccentricity cycle (124 and 95 ka). The Blackman-Tukey results (Fig. 4, C to E) also show that both before and after ~3.6 Ma BP, the strongest response corresponds approximately to eccentricity cycles (124, 121, and 106 ka). The intervals of 6.73 to 4.2 Ma BP and 4.2 to 2.58 Ma BP, separated by the monsoon precipitation shift at ~4.2 Ma BP, were also analyzed. Cycles of eccentricity (~122 ka), obliquity (~40 ka), and precession (~18 ka) are present during 2.58 to 4.2 Ma BP (fig. S5A), and an eccentricity cycle (~125 ka) is present during 4.2 to 6.73 Ma BP (fig. S5B). Probable half-precession cycles were detected before and after ~4.2 Ma BP (fig. S5).

To compare the climate response signal in the time series with Earth orbital variations, we filtered the 100-ka cycles of mean grain size and eccentricity (*23*). A comparison of the 100-ka band-pass filter results for the grain size and eccentricity time series is presented in Fig. 3 (E and F) (*16*). The two time series show similar phase patterns, indicating that the eccentricity and the monsoonal response were coupled from at least ~6.1 Ma BP. However, the amplitude of variation of the ~100-ka band in the monsoon records has a complex relationship with eccentricity: There is weak forcing but a strong precipitation response during 4.8 to 4.2 Ma BP and strong forcing but a weak precipitation response during 4.2 to 3.6 Ma BP. By contrast, both the forcing and the response were strongly coupled during 6.3 to 5.6 Ma BP (Fig. 3, E and F).

DISCUSSION

Paleoclimatic implications of variations in grain size and East Asian monsoon precipitation

Changes in the grain size composition of alluvial sediments can be attributed to three factors: changes in the sources of the clastic materials, lake-level fluctuations, and changes in hydrodynamics. The lithology of the CGC sections consists of sandy mudstone, siltstone, and sandstone, with similar mineral assemblages derived from a relatively small watershed, and therefore, the provenance has not substantially changed over time. Thus, there are two feasible interpretations of the grain size variations: (i) An increase in the >63-μm fraction in closed basins corresponds to a lower lake level and a smaller lake size and, hence, a drier climate or (ii) an increase in the >63-μm fraction reflects stronger precipitation and increased streamflow during an interval of wet climate. We favor the second interpretation for the following reasons: (i) From a geological perspective, the CGC section is located close to the Qinling Mountains, and the sediments have not been transported over long distances; therefore, the hydrodynamic power, an indication of precipitation intensity, will directly control the changes in grain size. Strong precipitation facilitates erosion and results in coarser grains being eroded from bedrock and transported to the depositional site. (ii) The >63-μm fraction comprises the major part of the deposits and it is positively correlated with the mean grain size (Fig. 3, A and B), suggesting that the grain size distributions are predominantly governed by streamflow dynamics. (iii) The sediments are mainly interbedded with brownish-red sandy mudstone and grayish-white coarse sandstone, which indicate oxidizing conditions and an open, shallow lake environment penetrated by fluvial systems. Therefore, it was not possible for large lake-level fluctuations to have occurred. Precipitation changes in the watershed are an important agent controlling the grain size distribution of sediments, especially in this monsoon-sensitive region. Given the co-occurrence of streamflow and monsoon precipitation, and that the monsoon history can be traced back to the Early Miocene (*24*) or even earlier (*16*, *25*), we conclude that, at least in the present context, the grain size can be used as a proxy for precipitation. During periods of increased monsoon rainfall, intensified stream runoff occurred, its erosional and sediment transport capacity increased,

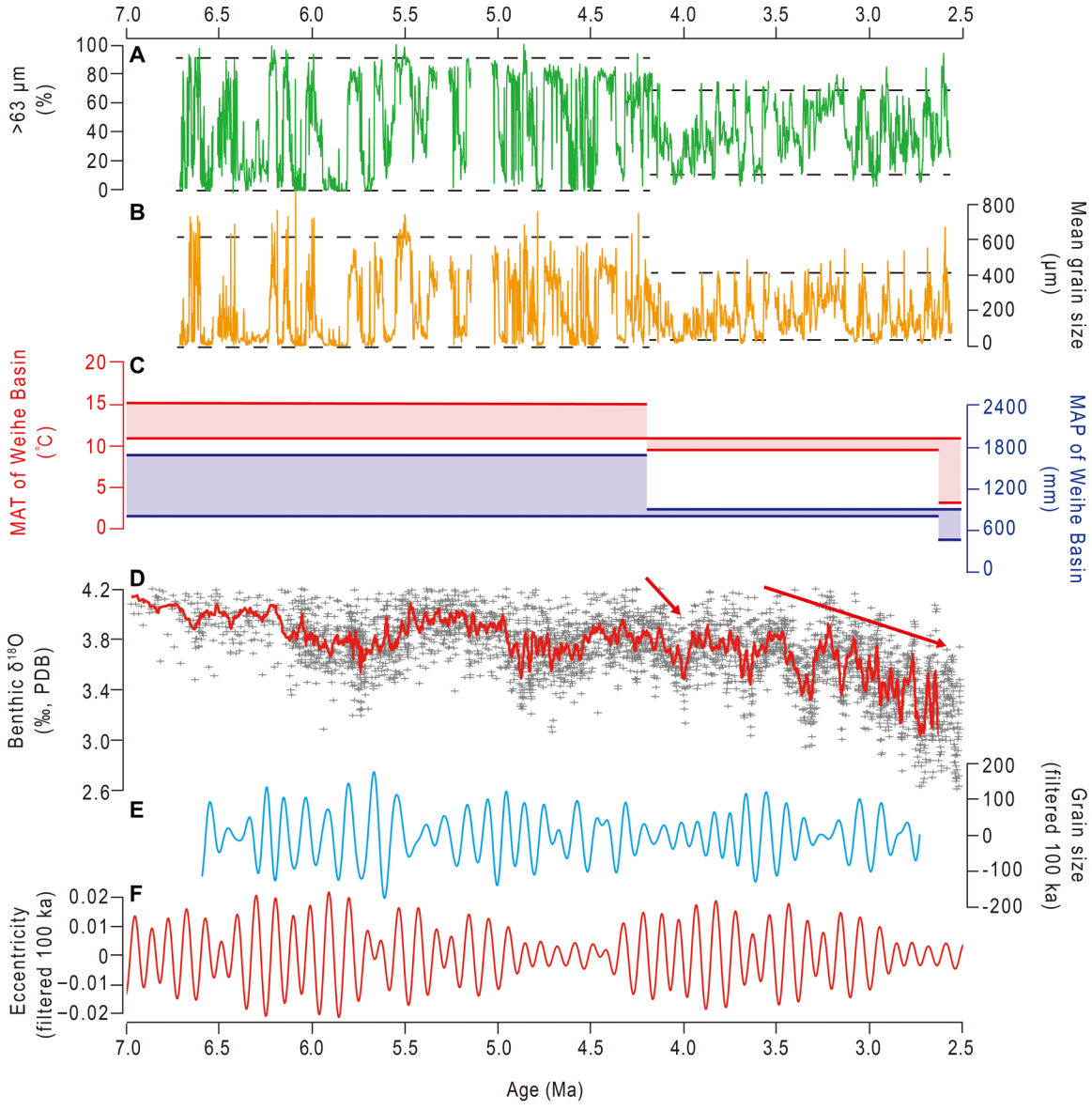

Fig. 3. East Asian monsoon precipitation during 6.73 to 2.58 Ma BP. (**A**) Grain size fraction of >63-μm (this study). (**B**) Mean grain size from this study. (**C**) MAT (mean annual temperature) and MAP (mean annual precipitation) of the Weihe Basin, from Wang *et al*. (*26*). (**D**) Global cooling trend recorded by the benthic $\delta^{18}O$ composite record of Zachos *et al*. (*11*). PDB, Pee Dee belemnite. (**E**) Band-pass filter of 100-ka of the mean grain size time series from this study. (**F**) Earth orbital eccentricity of 100 ka band-pass–filtered during 7.0 to 2.5 Ma BP from Laskar *et al*. (*23*).

coarser particles were carried to the basin, and the mean sedimentary grain size became coarser. Conversely, when the monsoon rainfall decreased, streamflow was reduced, fewer coarse particles were transported to the basin, and the sedimentary grain size became finer.

On this basis, the damped amplitude of the grain size time series indicates a step-like change in monsoon precipitation at ~4.2 Ma BP (Fig. 3, A and B). This decrease in monsoon precipitation is consistent with a lithological change (Fig. 2). Although changes in the local bed slopes could also lead to the lithological change, there is no clear evidence that tectonic deformation influenced the site and other contemporaneous Red Clay profiles nearby (*16*, *19*). Had there been a tectonically induced increase in bed slopes, there would have been more mélange deposits and possibly increased grain size variability within the sequence. The CGC section instead shows a damped amplitude of grain size variations and the less frequent occurrence of coarse-grained layers that suggest a step-like decrease in monsoon precipitation. This interpretation is in line with other proxy records from the region, which also show a climatic shift at ~4.2 Ma BP. For example, a recent phytolith-based quantitative reconstruction of monsoon precipitation in the area reveals a decrease in mean annual precipitation from ~800 to 1673 mm to ~443 to 900 mm at ~4.0 Ma BP (*26*). At the same time, a stepwise cooling occurred in the Weihe Basin [Fig. 3C; (*26*)] and elsewhere [Fig. 3D; (*11*)]. The Fe_2O_3 record of Red Clay deposits in the Chinese Loess Plateau indicates that the summer monsoon intensity was greatly reduced after a prolonged period of high intensity during 4.8 to 4.1 Ma BP (*27*) or 5.23 to 4.3 Ma BP (*28*).

We attribute the climatic shift at ~4.2 Ma BP to the cooling event in the high-latitude Northern Hemisphere (*11*, *29*), which predated

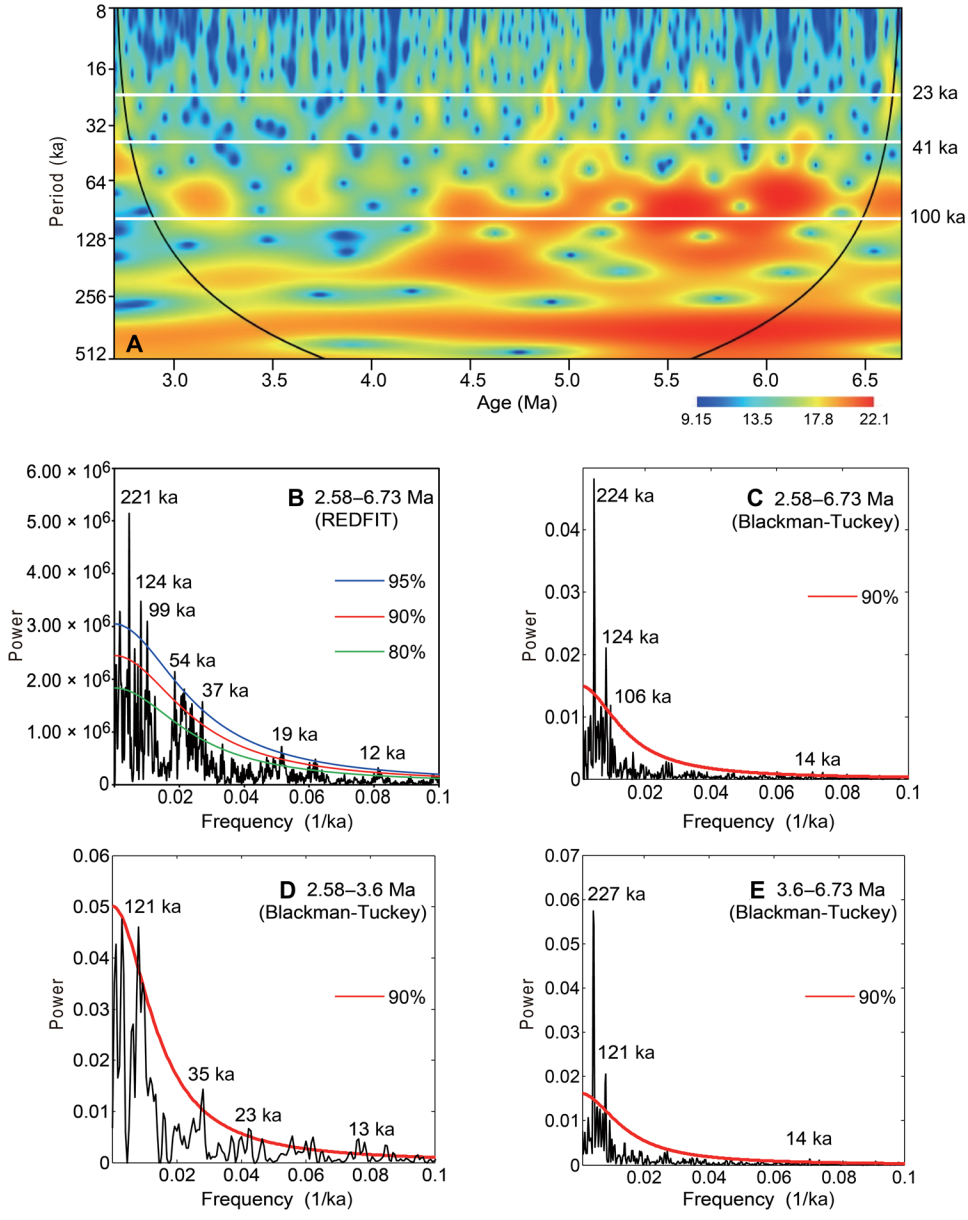

Fig. 4. Results of spectral analysis of East Asian monsoon precipitation variations during the Pliocene. (**A**) Wavelet analysis results of the mean grain size time series from this study; the reddish color indicates strong power, and the ~100-, ~41-, and ~20-ka periodicities are indicated by horizontal white lines. (**B**) REDFIT power spectrum analysis results for the interval of 2.58 to 6.73 Ma BP from this study. Blackman-Tukey spectrum analysis results of the mean grain size time series during 2.58 to 6.73 Ma BP (**C**), 2.58 to 3.4 Ma BP (**D**), and 3.4 to 6.73 Ma BP (**E**), from this study. The 80, 90, and 95% confidence levels are labeled with thick green, red, and blue lines, respectively.

the onset of NHG at ~3.6 Ma BP (*7*). Sea surface temperature (SST) data indicate a strengthened meridional SST gradient (*4*) and an intensified southward-penetrating cold tongue (*30*) at 4.0 to 4.3 Ma BP. A cooler Northern Hemisphere can increase the Pacific zonal SST gradient and strengthen the equatorial cold tongue, shifting the intertropical convergence zone (ITCZ) southward and thus affecting the Asian monsoon (*16*, *26*). Therefore, considering that the cooling and drying of the monsoon region occurred near-synchronously (Fig. 3), the decrease in precipitation at ~4.2 Ma BP was likely related to a threshold effect of the high-latitude cooling, via the migration of the ITCZ toward the tropical region, resulting in a narrowed monsoon precipitation belt and reduced monsoon precipitation in East Asia (*16*).

Variation in East Asian monsoon precipitation on the orbital scale and its forcing mechanism

The ~100-ka cycle is likely derived from insolation forcing, possibly through atmospheric CO_2 amplification of insolation forcing (*31*, *32*), and it is probably not governed by ice volume oscillations (*33*) or changes in ocean circulation (*34*). Notably, our record is not alone in revealing a climatic sensitivity to eccentricity forcing before the Pleistocene (*35*–*37*). The comparison between the monsoon response found in our time series and in Earth orbital variations indicates that the East Asian monsoon responded, albeit indirectly, to eccentricity forcing and that the two are well correlated, although with a mismatched amplitude of variation (Fig. 3, E and F). The fact that

the East Asian monsoon precipitation has been paced by eccentricity since at least 6.1 Ma BP implies its high sensitivity to external insolation forcing, while the amplitude mismatch points to the possible modulation by feedbacks internal to the climate system. A Southern Hemisphere influence through cross-equatorial moisture transport and latent heat release is a possible driver of variations in monsoon precipitation (*38*). Moreover, Rutherford and D'Hondt (*39*) pointed out that the increasing heat flow across the equator or the tropics to high latitudes can enhance the half-precession cycles in the Northern Hemisphere, resulting in the amplification of the ~100-ka signal. The strong presence of 12- to 14-ka cycles in our records (Fig. 4) supports this view.

In addition to the aforementioned orbital cycles, the ~221-ka signal (Fig. 4, B, C, and E) is likely an artifact of the grain size record in this particular section. The following causes are possible: (i) the interval at ~4.05 Ma BP, where there is a "missing" 100-ka peak; (ii) the missing ~100-ka peak at ~5.1 Ma BP, where there are missing data; (iii) the interval at ~5.9 Ma BP, where the grain size does not record an expected 100-ka peak; and (iv) the interval at ~6.3 Ma BP, where again the grain size does not record an expected 100-ka peak. These missing responses create the ~200-ka "cycle" in the spectrum. Three of the four instances occur in the older part of the section so that ~200-ka power is stronger than in the younger part of the record. These intervals correspond to grain size coarsening or shifts in sediment facies, showing that the sequence is not stable throughout the record, as would be expected in this type of depositional setting.

Previous investigations of East Asian monsoon variations during the Pliocene from both terrestrial [Red Clay deposits, (*40*)] and offshore marine records (*38*) indicate the possible orbital forcing of East Asian monsoon variations. However, the Red Clay has a low sedimentation rate and is susceptible to postdepositional weathering (*20*). For the offshore marine records, an independent time scale is still needed for the Pliocene interval. The obvious ~100-ka cycle as well as the ~40- and ~20-ka cycles present in the CGC record show that the East Asian monsoon responded to insolation in different ways in the Pliocene warm world and in the Pleistocene icehouse. Both the high- and low-latitude–dominated insolation bands appear in the monsoon precipitation time series, demonstrating both high- and low-latitude forcing of Asian monsoon evolution during the Pliocene. This differs from the findings of recent investigations of insolation forcing of Pleistocene monsoon variations (*1*), which are interpreted as a dominantly insolation-forced system.

Conclusions

Our records from the CGC sections in the Weihe Basin in Central China show that East Asian monsoon precipitation fluctuated at ~100-, ~40-, and ~20-ka cycles during the interval of 6.73 to 2.58 Ma BP. The presence of orbital cycles in a warm world with a high atmospheric CO_2 concentration and without Northern Hemisphere ice shows that insolation was crucial for modulating East Asian monsoon variations. The presence of precession and half-precession cycles in the monsoon record also indicates low-latitude forcing of East Asian monsoon variability. Our finding of a ~4.2-Ma BP monsoon shift in the CGC section is interpreted to reflect a threshold response to Northern Hemisphere high-latitude cooling, perhaps via atmospheric circulation and oceanic currents, which narrowed the extent of the ITCZ, reducing the precipitation in this monsoon-sensitive region. Our results also suggest that climate signals originating in both high and low latitudes drove East Asian monsoon variations during the Pliocene warm period.

MATERIALS AND METHODS

Magnetostratigraphy

A total of 650 oriented paleomagnetic samples were taken from a 268.5-m interval of the CGC section, at intervals of 0.2 to 0.5 m (1 to 5 m in the coarse sandstone and conglomerate parts), after removal of the weathered surface material of the outcrops. A total of 500 samples were cut into 2 cm by 2 cm by 2 cm cubes and thermally demagnetized using a TD-48 thermal demagnetizer and measured with a 2G superconducting magnetometer housed in the magnetically shielded room in the Paleomagnetism Laboratory of Nanjing University. Progressive thermal demagnetization was carried out up to 690°C for most samples, with more than 19 temperature steps with an increment of 50°C for temperatures below 550°C and with steps of 20° to 30°C for temperatures above 550°C, comprising the Curie temperature points of major ferrimagnetic minerals.

Below 250°C, the magnetization is dominated by a secondary overprint (fig. S6). This secondary remanence was gradually removed with increasing demagnetization temperature. From 250° to 680°C, the ChRM was isolated and is represented by a relatively unidirectional trajectory toward the origin. The NRM intensity was typically of the order of 10^{-4} to 10^{-2} A/m. In most samples, a gradual remanence decay occurred from 250° to 680°C, with a drop near the Curie temperature of magnetite (~580°C), indicating the presence of magnetite. The remanence of most of the samples was reduced to near zero at 670° to 680°C, indicating that hematite (Curie temperature of 675°C) is an important magnetic carrier.

The demagnetization results were subsequently evaluated using orthogonal vector demagnetization diagrams (*41*), and the ChRM was determined by principal components analysis (*42*). A ChRM is defined using the demagnetization data at several demagnetization steps (usually four to eight steps) with temperature ranges between 250° and 680°C. The ChRM directions (fig. S7) show both normal and reserved polarities. A reversal test was performed using PaleoMac software (*43*), passing at the 95% confidence level with class "B" (*44*). The reliable ChRMs were then used to establish the magnetic polarity sequence. The declination (Dec) and inclination (Inc) of selected samples (maximum angular deviation, <15°), together with the geographical location of the sampling section, were used to calculate the VGP latitude to establish the magnetic polarity stratigraphy (Fig. 2).

Grain size and magnetic susceptibility

The grain size of 2549 bulk samples was analyzed using a Malvern Mastersizer 2000 particle size analyzer (analytical range of 0.02 to 2000 μm). The samples were pretreated with hot H_2O_2 to remove organic matter and then with HCl to remove carbonate, following standard procedures, in the Laboratory of Earth Surface Processes and Environment in Nanjing University.

The magnetic susceptibility of 2549 powdered samples was measured using a Bartington magnetic susceptibility meter. Approximately 10 g of each sample was dried at temperatures below 38°C and measured three times; the average was then used to reduce errors.

Spectral analysis

To detect cycles within the grain size time series, a continuous wavelet transform was carried out using PAST3 software (*45*). Before wavelet analysis, the unevenly spaced data were interpolated to a 1.6-ka time step. To test whether peaks in the spectrum were significant against the red-noise background, we first performed REDFIT (*46*) analysis (rectangular window) on the unevenly spaced data and

then interpolated these data to 1.6-ka intervals to conduct Blackman-Tukey spectral analysis to further verify the robustness of the cycles.

SUPPLEMENTARY MATERIALS

Supplementary material for this article is available at http://advances.sciencemag.org/cgi/content/full/6/46/eabc2414/DC1

REFERENCES AND NOTES

1. H. Cheng, R. L. Edwards, A. Sinha, C. Spötl, L. Yi, S. Chen, M. Kelly, G. Kathayat, X. Wang, X. Li, X. Kong, Y. Wang, Y. Ning, H. Zhang, The Asian monsoon over the past 640,000 years and ice age terminations. *Nature* **534**, 640–646 (2016).
2. S. C. Clemens, A. Holbourn, Y. Kubota, K. E. Lee, Z. Liu, G. Chen, A. Nelson, B. Fox-Kemper, Precession-band variance missing from east Asian monsoon runoff. *Nat. Commun.* **9**, 3364 (2018).
3. K. D. Burke, J. W. Williams, M. A. Chandler, A. M. Haywood, D. J. Lunt, B. L. Otto-Bliesner, Pliocene and Eocene provide best analogs for near-future climates. *Proc. Natl. Acad. Sci. U.S.A.* **115**, 13288–13293 (2018).
4. C. M. Brierley, A. V. Fedorov, Z. Liu, T. D. Herbert, K. T. Lawrence, J. P. LaRiviere, Greatly expanded tropical warm pool and weakened hadley circulation in the early Pliocene. *Science* **323**, 1714–1718 (2009).
5. A. C. Ravelo, D. H. Andreasen, M. Lyle, A. O. Lyle, M. W. Wara, Regional climate shifts caused by gradual global cooling in the Pliocene epoch. *Nature* **429**, 263–267 (2004).
6. S. De Schepper, P. L. Gibbard, U. Salzmann, J. Ehlers, A global synthesis of the marine and terrestrial evidence for glaciation during the Pliocene Epoch. *Earth Sci. Rev.* **135**, 83–102 (2014).
7. M. Mudelsee, M. E. Raymo, Slow dynamics of the Northern Hemisphere glaciation. *Paleoceanography* **20**, PA4022 (2005).
8. G. H. Haug, A. Ganopolski, D. M. Sigman, A. Rosell-Mele, G. E. A. Swann, R. Tiedemann, S. L. Jaccard, J. Bollmann, M. A. Maslin, M. J. Leng, G. Eglinton, North Pacific seasonality and the glaciation of North America 2.7 million years ago. *Nature* **433**, 821–825 (2005).
9. T. D. Herbert, K. T. Lawrence, A. Tzanova, L. C. Peterson, R. Caballero-Gill, C. S. Kelly, Late Miocene global cooling and the rise of modern ecosystems. *Nat. Geosci.* **9**, 843–847 (2016).
10. C. Karas, N. Khelif, A. Bahr, B. D. A. Naafs, D. Nürnberg, J. O. Herrle, Did North Atlantic cooling and freshening from 3.65–3.5 Ma precondition Northern Hemisphere ice sheet growth? *Global Planet. Change* **185**, 103085 (2020).
11. J. C. Zachos, G. R. Dickens, R. E. Zeebe, An early Cenozoic perspective on greenhouse warming and carbon-cycle dynamics. *Nature* **451**, 279–283 (2008).
12. L. E. Lisiecki, M. E. Raymo, A Pliocene-Pleistocene stack of 57 globally distributed benthic $\delta^{18}O$ records. *Paleoceanography* **20**, PA1003 (2005).
13. Institute of Vertebrate Paleontology and Paleoanthropology, *Symposium of the Field Conference of Cenozoic of Lantian, Shaanxi* (Chinese Academy of Sciences, 1966)
14. A. Kaakinen, J. P. Lunkka, Sedimentation of the Late Miocene Bahe Formation and its implications for stable environments adjacent to Qinling Mountains in Shaanxi, China. *J. Asian Earth Sci.* **22**, 67–78 (2003).
15. A. Kaakinen, A long terrestrial sequence in Lantian– a window into the late Neogene palaeoenvironments of northern China, thesis, University of Helsinki, Publications of the Department of Geology (2005), pp. 49.
16. H. Lu, H. Z. Zhang, Y. Wang, L. Zhao, H. Wang, W. Sun, H. Y. Zhang, Cenozoic depositional sequence in the Weihe Basin (Central China): A long-term record of Asian monsoon precipitation from the greenhouse to icehouse earth. *Quat. Sci.* **38**, 1057–1067 (2018).
17. Y. Zhang, W. Huang, Y. Tang, H. Ji, Y. You, Y. Tong, S. Ding, X. Huang, J. Zheng, *Cenozoic Stratigraphy of the Lantian Region, Shaanxi Province* (Science Press, 1978).
18. Z. L. Ding, S. F. Xiong, J. M. Sun, S. L. Yang, Z. Y. Gu, T. S. Liu, Pedostratigraphy and paleomagnetism of a ~7.0 Ma eolian loess–red clay sequence at Lingtai, Loess Plateau, north-central China and the implications for paleomonsoon evolution. *Palaeogeogr. Palaeoclimatol. Palaeoecol.* **152**, 49–66 (1999).
19. Z. An, D. Sun, M. Chen, Y. Sun, L. Li, B. Chen, Red clay sequences in Chinese loess plateau and recorded paleoclimate events of the late Tertiary. *Quat. Sci.* **20**, 435–446 (2000).
20. H. Lu, X. Wang, L. Li, Aeolian sediment evidence that global cooling has driven late Cenozoic stepwise aridification in central Asia. *Geol. Soc. London Spec. Publ.* **342**, 29–44 (2010).
21. J. G. Ogg, Geomagnetic polarity time scale, in *The Geologic Time Scale* (Cambridge Univ. Press, ed. 1, 2012), pp. 85–113.
22. B. Wang, Cenozoic Sedimentary Evolution of the Weihe Basin: Basin-Orogen Coupling and Eolian Sediments, thesis, Nanjing University (2014), pp. 109.
23. J. Laskar, P. Robutel, F. Joutel, M. Gastineau, A. C. M. Correia, B. Levrar, A long-term numerical solution for the insolation quantities of the Earth. *Astron. Astrophys.* **428**, 261–285 (2004).
24. Z. T. Guo, W. F. Ruddiman, Q. Z. Hao, H. B. Wu, Y. S. Qiao, R. X. Zhu, S. Z. Peng, J. J. Wei, B. Y. Yuan, T. S. Liu, Onset of Asian desertification by 22 Myr ago inferred from loess deposits in China. *Nature* **416**, 159–163 (2002).
25. A. Licht, M. van Cappelle, H. A. Abels, J.-B. Ladant, J. Trabucho-Alexandre, C. France-Lanord, Y. Donnadieu, J. Vandenberghe, T. Rigaudier, C. Lécuyer, D. Terry Jr., R. Adriaens, A. Boura, Z. Guo, A. N. Soe, J. Quade, G. Dupont-Nivet, J.-J. Jaeger, Asian monsoons in a late Eocene greenhouse world. *Nature* **513**, 501–506 (2014).
26. H. Wang, H. Lu, L. Zhao, H. Zhang, F. Lei, Y. Wang, Asian monsoon rainfall variation during the Pliocene forced by global temperature change. *Nat. Commun.* **10**, 5272 (2019).
27. Z. Ding, S. Yang, J. Sun, T. Liu, Iron geochemistry of loess and red clay deposits in the Chinese Loess Plateau and implications for long-term Asian monsoon evolution in the last 7.0 Ma. *Earth Planet Sci. Lett.* **185**, 99–109 (2001).
28. S. Yang, Z. Ding, S. Feng, W. Jiang, X. Huang, L. Guo, A strengthened East Asian Summer Monsoon during Pliocene warmth: Evidence from 'red clay' sediments at Pianguan, northern China. *J. Asian Earth Sci.* **155**, 124–133 (2018).
29. G. H. Haug, R. Tiedemann, Effect of the formation of the Isthmus of Panama on Atlantic Ocean thermohaline circulation. *Nature* **393**, 673–676 (1998).
30. J. Liu, J. Tian, Z. Liu, T. D. Herbert, A. V. Fedorov, M. Lyle, Eastern equatorial pacific cold tongue evolution since the late Miocene linked to extratropical climate. *Sci. Adv.* **5**, eaau6060 (2019).
31. N. J. Shackleton, The 100,000-year ice-age cycle identified and found to lag temperature, carbon dioxide, and orbital eccentricity. *Science* **289**, 1897–1902 (2000).
32. D. W. Lea, The 100 000-yr cycle in tropical SST, greenhouse forcing, and climate sensitivity. *J. Climate* **17**, 2170–2179 (2004).
33. J. Imbrie, A. Berger, E. A. Boyle, S. C. Clemens, A. Duffy, W. R. Howard, G. Kukla, J. Kutzbach, D. G. Martinson, A. McIntyre, A. C. Mix, B. Molfino, J. J. Morley, L. C. Peterson, N. G. Pisias, W. L. Prell, M. E. Raymo, N. J. Shackleton, J. R. Toggweiler, On the structure and origin of major glaciation cycles 2. The 100,000-year cycle. *Paleoceanography* **8**, 699–735 (1993).
34. J. R. Toggweiler, Origin of the 100,000-year timescale in Antarctic temperatures and atmospheric CO_2. *Paleoceanography* **23**, PA2211 (2008).
35. S. C. Clemens, R. Tiedemann, Eccentricity forcing of Pliocene–early Pleistocene climate revealed in a marine oxygen-isotope record. *Nature* **385**, 801–804 (1997).
36. J. C. Zachos, B. P. Flower, H. Paul, Orbitally paced climate oscillations across the Oligocene/Miocene boundary. *Nature* **388**, 567–570 (1997).
37. M. L. Lantink, J. Davies, P. R. D. Mason, U. Schaltegger, F. J. Hilgen, Climate control on banded iron formations linked to orbital eccentricity. *Nat. Geosci.* **12**, 369–374 (2019).
38. S. C. Clemens, W. L. Prell, Y. Sun, Z. Liu, G. Chen, Southern Hemisphere forcing of Pliocene $\delta^{18}O$ and the evolution of Indo-Asian monsoons. *Paleoceanography* **23**, PA4210 (2008).
39. S. Rutherford, S. D'Hondt, Early onset and tropical forcing of 100,000-year Pleistocene glacial cycles. *Nature* **408**, 72–75 (2000).
40. Y. Sun, Z. An, S. C. Clemens, J. Bloemendal, J. Vandenberghe, Seven million years of wind and precipitation variability on the Chinese Loess Plateau. *Earth Planet. Sci. Lett.* **297**, 525–535 (2010).
41. J. D. A. Zijderveld, A. C. demagnetization of rocks: Analysis of results. *Dev. Solid Earth Geophys.* **3**, 254–286 (2013).
42. J. L. Kirschvink, The least-squares line and plane and the analysis of palaeomagnetic data. *Geophys. J. Int.* **3**, 699–718 (1980).
43. J. P. Cogné, PaleoMac: A Macintosh application for treating paleomagnetic data and making plate reconstructions. *Geochem. Geophys. Geosyst.* **4**, 1007 (2003).
44. P. L. McFadden, M. W. McElhinny, Classification of the reversal test in palaeomagnetism. *Geophys. J. Int.* **103**, 725–729 (1990).
45. Ø. Hammer, D. A. T. Harper, P. D. Ryan, PAST: Paleontological statistics software package for education and data analysis. *Palaeontologia Electronica* **4**, 9 (2001).
46. M. Schulz, M. Mudelsee, REDFIT: Estimating red-noise spectra directly from unevenly spaced paleoclimatic time series. *Comput. Geosci. UK* **28**, 421–426 (2002).
47. J. V. Waters, S. J. Jones, H. A. Armstrong, Climatic controls on late Pleistocene alluvial fans, Cyprus. *Geomorphology* **115**, 228–251 (2010).
48. S. P. Todd, Stream-driven, high-density gravelly traction carpets: Possible deposits in the Trabeg conglomerate formation, SW Ireland and some theoretical considerations of their origin. *Sedimentology* **36**, 513–530 (1989).
49. R. A. Buckley, A. G. Plint, O. A. Henderson, J. R. Krawetz, K. M. Vannelli, Ramp sedimentation across a middle Albian, Arctic embayment: Influence of subsidence, eustasy and sediment supply on stratal architecture and facies distribution, Lower Cretaceous, Western Canada Foreland Basin. *Sedimentology* **63**, 699–742 (2016).

Acknowledgments: We thank Z. Zhang for help with identifying the fossils within the section and J. Wan, M. Wang, Z. Huang, L. Zhao, H. Zhang, Y. Li, X. Chang, Y. Gu, C. Liang, S. Wang, and L. Cheng for assistance in the field. We thank D. Lea and two reviewers for helpful and constructive comments. **Funding:** This research is supported by the National Natural Science Foundation of China (41888101, 41690111, and 41920104005). **Author contributions:** H.Lu

designed and organized this study. H.Lu, Yichao Wang, K.W., H.Lv, H.W., F.L., Z.H., and H.Z. performed the fieldwork. Yichao Wang, K.W., H.Lv, Z.H., Y.L., and X.H. carried out the laboratory analysis. Yao Wang undertook the spectral analysis. Yichao Wang and H.Lu wrote the manuscript. Y.L. and S.C. revised the manuscript. All the authors discussed and contributed to the manuscript. **Competing interests:** The authors declare that they have no competing interests. **Data and materials availability:** All data needed to evaluate the conclusions in the paper are present in the paper and/or the Supplementary Materials. Additional data related to this paper may be requested from the corresponding author.

Submitted 14 April 2020
Accepted 30 September 2020
Published 13 November 2020
10.1126/sciadv.abc2414

Citation: Y. Wang, H. Lu, K. Wang, Y. Wang, Y. Li, S. Clemens, H. Lv, Z. Huang, H. Wang, X. Hu, F. Lu, H. Zhang, Combined high- and low-latitude forcing of East Asian monsoon precipitation variability in the Pliocene warm period. *Sci. Adv.* **6**, eabc2414 (2020).